Multi-objective model predictive control method for T-type three-level grid-connected

Ning Pan [1], Zhen Xie[2], Jiaqing Mo[1*], Yuanhao Wang[1]

[1]Xinjiang Key Laboratory of Signal Detection and Processing, School of Information Science and Engineering, Xinjiang University, Urumqi 830017, China
[2]Dongguan Guangya intelligent technology Co., LTD, Dongguan China

Abstract. Based on the mathematical model of T-type three-level topology, a T-type three-level inverter model is proposed to predict the multi-objective control method, which mainly includes DC neutral voltage (NP-V), switching state, inverter voltage vector, and multi-objective cost function. Different emphases can be selected according to the application requirements, and coordinated control of different control objectives can be realized by giving different weight values to different control objectives. An extended observer (ESO) is added to observe the error part of the grid-connected inverter system, and the observed results are compensated to the grid-connected reference voltage. The simulation results show that the total harmonic distortion rate of the output current of the inverter is lower than that of the traditional finite control set model predictive control strategy. In addition, the proposed method can realize the balance control of the midpoint potential, and the principle is simple.

1 Introduction

With the rapid development of renewable distributed new energy technologies such as wind energy and solar energy, grid-connected inverters have become a research hotspot in the field of power electronics. Grid-connected inverters play an important role in processing the DC generated by renewable energy and transmitting it to the power grid[1].

In the application field of high-voltage and high-power inverters, compared with two-level converters, three-level converters with three-level midpoint clamp topology have been widely used due to their advantages of simple structure, fewer devices, low voltage stress, and high output voltage and current quality [2-3]. In reference [4], the geometric analysis method is used to prove that the performance of T-type three-level converter is better than that of NPC converter. Among many three-phase inverters, compared with mid-point clamp inverters, T-type three-level three-phase inverters can reduce 6 power diodes, and can improve the conversion efficiency in the switching frequency range of 5-30 kHz [5-6].

In inverter Control strategies, such as PI double closed-loop control [7], active disturbance rejection control and sliding mode variable structure control [8], Model Predictive Control (MPC) has gradually developed and matured, and model predictive control has fast dynamic response and flexible control objectives. It has become an important research branch in the field of control [9-10]. Reference [11] proposes to apply FCS-MPC control to more high-level topologies to improve inverter efficiency. The steps of MPC execution are described in detail in reference [12].

This paper presents a multi-objective model predictive control strategy for T-type three-level inverter, which can realize the coordinated control of different targets according to different weights and make its application more extensive.

2 Model T Three-Level Inverter System Modeling and Model Predictive Control Principle

2.1. T-type three-level system model

Figure 1 shows the structure of T-type three-level converter, which is powered by DC power supply Udc and connected to the power grid through LC filter on the output side, including DC capacitor C1, C2 and 12 switching devices. The switching signal of the switching tube is defined as.

$$s_{xn} = \begin{cases} 1 & \text{close} \\ 0 & open \end{cases} \quad \text{x} \in \{\text{a,b,c}\}, \text{n} \in \{1,2,3,4\} \quad (1)$$
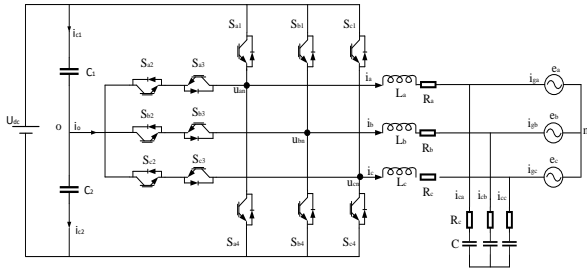
Figure 1. structure of T-type three-level inverter.

Each item of the converter switches the output P, O, N three states according to the switching device, a total of 3^2=27 switching states. The space voltage vector of T-type Three-level Inverter is as shown in Fig. 2. Take phase A as an example. While Sa1 and Sa2 are closed (ON), but Sa3 and Sa4 are OFF, the switch is at P status; when Sa2 and Sa3 are closed, but Sa1 and Sa4 are OFF, the switch is at O status; when Sa3 and Sa4 are closed, but Sa1 and Sa2 are OFF, the switch is at N status.

The corresponding relationship between the output voltage and the voltage space state of the inverter is shown in Table 1, and the corresponding relationship between the voltage space state and the DC capacitance charge and discharge is shown in Table 2. From Table 2, it can be seen that the NP-V is not affected by the action of large vector and zero vector. Medium vector and small vector will cause the fluctuation of the midpoint potential, in which the pairs of positive and negative small vectors cancel each other, and have no effect on the midpoint voltage.

Table 1. The correspondence between the spatial vector of the T-type three-level inverter and the switching state

S_a	S_b	S_c	V_i
N	N	N	V_0=0
O	N	N	V_1=(1/3)U_{dc}
O	O	N	V_2=(1/6)U_{dc}+j($\sqrt{3}$/6)U_{dc}
N	O	N	V_3=-(1/6)U_{dc}+j($\sqrt{3}$/6)U_{dc}
N	O	O	V_4=-(1/3)U_{dc}
N	N	O	V_5=-(1/6)U_{dc}-j($\sqrt{3}$/6)U_{dc}
O	N	O	V_6= (1/6)U_{dc}-j($\sqrt{3}$/6)U_{dc}
O	O	O	V_7=0
P	O	O	V_8=(1/3)U_{dc}
P	P	O	V_9=(1/6)U_{dc}+j($\sqrt{3}$/6)U_{dc}
O	P	O	V_{10}=-(1/6)U_{dc}+j($\sqrt{3}$/6)U_{dc}
O	P	P	V_{11}=-(1/3)U_{dc}
O	O	P	V_{12}=-(1/6)U_{dc}-j($\sqrt{3}$/6)U_{dc}
P	O	P	V_{13}= (1/6)U_{dc}-j($\sqrt{3}$/6)U_{dc}
P	P	P	V_{14}=0
P	N	N	V_{15}=(2/3)U_{dc}
P	O	N	V_{16}=(1/2)U_{dc}+j($\sqrt{3}$/6)U_{dc}
P	P	N	V_{17}=(1/3)U_{dc}+j($\sqrt{3}$/3)U_{dc}
O	P	N	V_{18}=j($\sqrt{3}$/3)U_{dc}
N	P	N	V_{19}=-(1/3)U_{dc}+j($\sqrt{3}$/3)U_{dc}

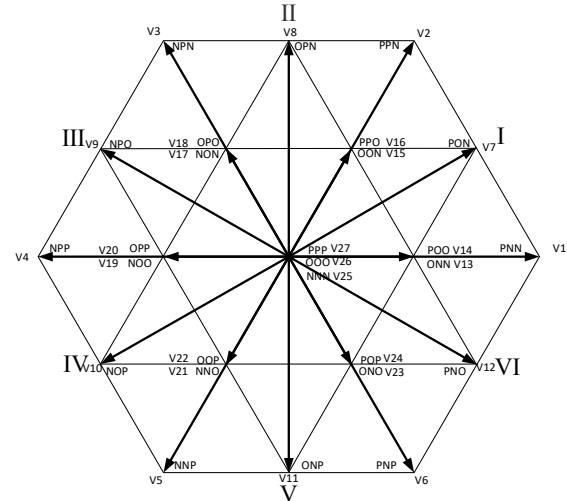| N	P	O	V_{20}=-(1/2)U_{dc}+j($\sqrt{3}$/6)U_{dc}
N	P	P	V_{21}=-(2/3)U_{dc}
N	O	P	V_{22}=-(1/2)U_{dc}-j($\sqrt{3}$/6)U_{dc}
N	N	P	V_{23}=-(1/2)U_{dc}-j($\sqrt{3}$/6)U_{dc}
O	N	P	V_{24}=-j($\sqrt{3}$/3)U_{dc}
P	N	P	V_{25}= (1/3)U_{dc}-j($\sqrt{3}/3$)U_{dc}
P	N	O	V_{26}= (1/2)U_{dc}-j($\sqrt{3}$/6)U_{dc}

Figure 2. Spatial voltage vector of T-type three-level inverter

Table 2. Spatial voltage vector of T-type three-level inverter.

On-off state	i_o	Dc bus capacitance status
POO	-i_a	
PPO	i_c	
OPO	-i_b	C_1 Electric discharge
OPP	i_a	C_2 charging
OOP	-i_c	
POP	i_b	
ONN	i_a	
OON	-i_c	
NON	i_b	C_1 charging
NOO	-i_a	C_2 Electric discharge
NNO	i_c	
ONO	-i_b	

2.2. T-type three-level predictive control principle

According to the current reference direction in Figure 1, the dynamic model of the inverter is established in the static coordinate system as

$$u_{xn} = L_x \frac{di_x}{dt} + R_x i_x + e_x \quad x \in (a, b, c) \tag{2}$$

In formula (2), uxn is the output voltage of the inverter, ex is the grid voltage, and ix is the flowing inductive current.

In formula (2), the simplified model of the system in the αβ rotating coordinate system obtained by Clarke transformation is as follows:

$$u_{\alpha\beta} = L_s \frac{di_{\alpha\beta}}{dt} + R_s i_{\alpha\beta} + e_{\alpha\beta} \tag{3}$$

Formula (4) is obtained by forward Euler discretization of formula (3):

$$i_{\alpha\beta}(k+1) = i_{\alpha\beta}(k) + \frac{T_s}{L_s}(e_{\alpha\beta}(k) - u_{\alpha\beta}(k) - R_s i_{\alpha\beta}(k)) \quad (4)$$

The problem of neutral point potential balance on the DC side is a problem that cannot be solved in all three-level topologies, and the partial voltage of the two series capacitors on the DC side must be approximately the same[13].

The main reasons for the imbalance of Neutral potential balance are as follows :1) the switch action signal is delayed, resulting in the imbalance of midpoint potential; 2) The inflow and outflow of the DC capacitor midpoint current is the main reason for the imbalance of midpoint potential; 3) The active and reactive current components also cause an imbalance.

Hazards of unbalance of midpoint potential:1) When the inverter is connected to the grid, the voltage distorts and the midpoint potential shifts are aggravated.2) It can also cause damage to the switching device.

The DC capacitor voltage can be described as

$$\begin{cases} \dfrac{du_{c1}}{dt} = \dfrac{1}{C}i_{c1} \\ \dfrac{du_{c2}}{dt} = \dfrac{1}{C}i_{c2} \end{cases} \quad (5)$$

The equation (5) is obtained by forward Eulerian discretization:

$$\begin{cases} u_{c1}(k+1) = u_{c1}(k) + \dfrac{1}{C}i_{c1}(k)T_s \\ u_{c2}(k+1) = u_{c2}(k) + \dfrac{1}{C}i_{c2}(k)T_s \end{cases} \quad (6)$$

The currents iC1(k) and iC2(k) are related to the switching state and output current value of the inverter and can be calculated by the following expression

$$\begin{cases} i_{C1}(k) = i_{dc}(k) - H_{1a}i_a(k) - H_{1b}i_b(k) - H_{1c}i_c(k) \\ i_{C2}(k) = i_{dc}(k) + H_{2a}i_a(k) + H_{2b}i_b(k) + H_{2c}i_c(k) \end{cases} \quad (7)$$

The idc in formula (7) is the current generated by the DC voltage source Udc.

Current iC1 (k) and iC2 (k) are related to the switching state and output current value of the inverter, and can be expressed as

$$\begin{cases} H_{1x} = \begin{cases} 1, & S_x=2 \\ 0, & others \end{cases} \\ H_{2x} = \begin{cases} 1, & S_x=0 \\ 0, & others \end{cases} \end{cases} (x \in a,b,c) \quad (8)$$

2.3. Cost function design

In the finite set model predictive control algorithm, the design idea of value function is the core part of the whole control algorithm design, and different value function design will produce completely different control effects on the system state variables. Multi-objective predictive control method can put different control variables into a value function and give different weights to different targets to achieve coordinated control of different targets. In this paper, grid voltage, midpoint voltage, and changes before and after switching state are added to the voltage control algorithm of value function predictive control

$$g = |u_{ref\alpha}(k) - u_\alpha(k)| + |u_{ref\beta}(k) - u_\beta(k)| + |\lambda_1(u_{c1}(k+1) - u_{c2}(k+1))^2 + \lambda_2 n| \quad (9)$$

λ1 and λ2 are the weight coefficients, and their values determine the priority of the controlled variable in the whole world. The accurate control of current tracking and midpoint balance in the T-type three-level converter is achieved by setting λ, and n is the change value before and after the three-phase switching state.

3 Model error compensation

3.1. Inverter dynamic motion model considering model error

Assume that there are deviations ΔLx and ΔRx in inductance and resistance between the actual system and the predicted system, where x ∈ "{a,b,c}". The actual model of the system can be derived from formula (2)

$$\frac{di_x}{dt} = \frac{u_{refxn}}{L_x} - \frac{R_x i_x}{L_x} - \frac{e_x}{L_x} + \Delta L_x \frac{di_x}{dt} + \Delta R_x i_x \quad (10)$$

The inverter current loop is a first-order nonlinear system, so that the voltage error generated by parameter mismatch is the internal unknown disturbance f(ix)=(ΔLxdix/dt+ΔRxix), the external voltage disturbance Nx(t)=-ex, and the control gain is Jx=1/Lx

$$\frac{di_x}{dt} = j_x(f(i_x) + N_x(t) + u_{refxn}) \quad (11)$$

With the reference voltage on the grid side as system input uxs, ix as system output yx, ix as state variable x1, the first-order system is constructed as

$$\begin{cases} x_1 = j_x(f(x_1) + N_x(t) + u_{xs}) \\ y_x = x_1 \end{cases} \quad (12)$$

Let the generalized perturbation x2=ax(x1)=jxfx(ix)+jxNx(t), build the system as

$$\begin{cases} \dot{x}_1 = x_2 + j_x u_{xs} \\ \dot{x}_2 = f_x(i_x) + j_x(t) \\ y_x = x_1 \end{cases} \quad (13)$$

3.2. Build an expansion observer in an inverter

The extended observer estimates the state variables x1 and x2 according to the input values urefxn and output values ix of the system, and then realizes dynamic disturbance feedforward compensation. For the above formula, the ESO is established as

$$\begin{cases} e_x = Z_{x1} - x_1 \\ \dot{Z}_{x2} = Z_{x2} - \beta_1 e_{x1} + j_x u_{xs} \\ \dot{Z}_{x2} = -\beta_2 e_{x1} \end{cases} \quad (14)$$

The values of ESO modulation coefficients β1 and β2 can be determined after several debugging. Finally, by adding the observation results to formula (15), the

reference voltage U*refx(k) on the grid side after k time compensation can be obtained as

$$u^*_{refx}(k) = \frac{L_x}{T_s} i_{refx}(k+1) + (R_x - \frac{L_x}{T_s}) i_x(k) + e_x(k) + Z_2 \quad (15)$$

# 4 Simulation verification

4.1. System parameter

Based on the above theoretical analysis, a simulation analysis of a T-type three-level inverter was conducted using Matlab/Simulink. The main parameters are shown in the table 3 below:

Table 3. System parameter

Description and Symbol	Value
DC side voltage,Udc	800V
Grid side phase voltage,e	220V
Grid frequency,f	50Hz
Dc capacitance,C1,C2	470uF
LC filter inductor,L	8mH
LC filter capacitance,C	10uf
L parasitic resistance,Rs	0.02Ω
Sampling period,Ts	0.05ms

The output performance of converters with different control strategies is analyzed and compared. The traditional FCS-MPC is λ=0.5, and the multi-objective finite set MPC algorithm is λ1=0.5 at the DC midpoint potential balance and λ2=0.1 at the switching state optimization are simulated respectively. FCS-MPC is set as strategy A and multi-objective control strategy as strategy B. FIG. 3 and FIG. 4 show the output voltage and current of the converters of the two algorithms. The RMS value of the given three-phase reference current is 15A. Combined with the implementation analysis, the output current ripple of the B control algorithm is smaller and the voltage utilization rate is higher.

Figure 5 shows the total harmonic distortion rate of the output current of the inverter, and Figure (e) and (f) respectively show the THD of the output current of the inverter. It can be analyzed from the figure that the THD of the output current of the converter side is reduced from the original 2.20% to 0.76%, which improves the power quality of the current incorporated into the grid.
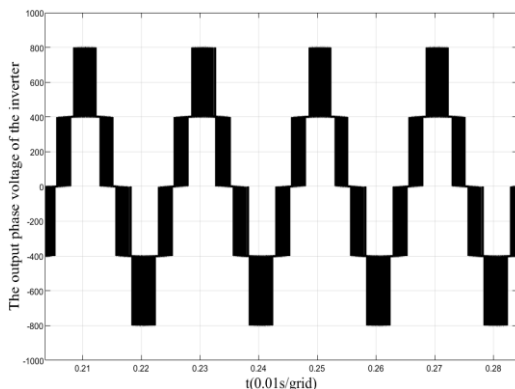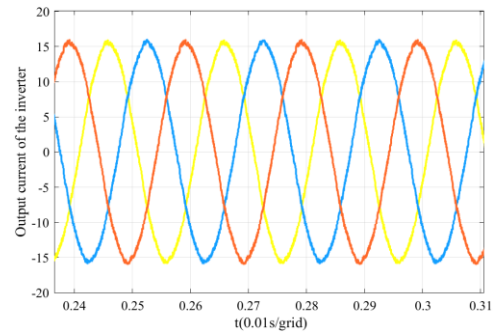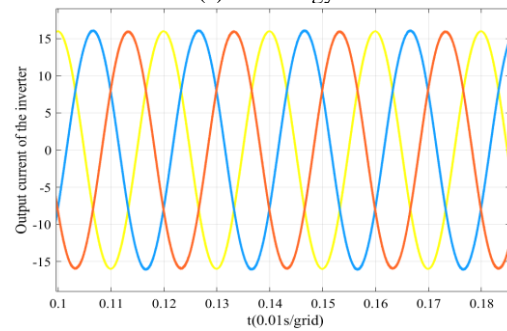
(a). A strategy
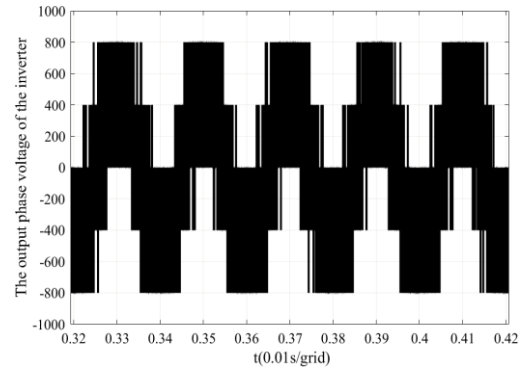
(b). B strategy

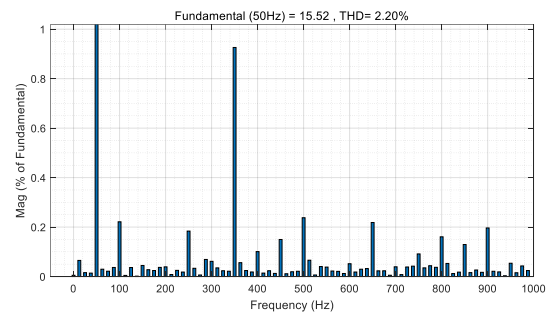**Figure 3.** Inverter output side phase voltage.
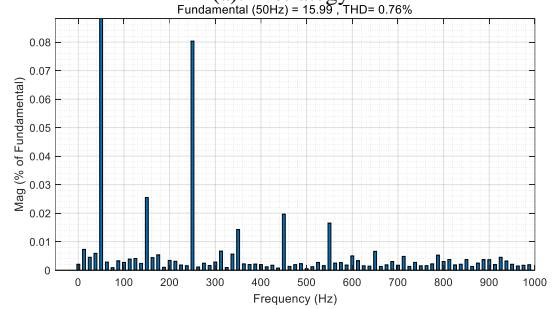
(a). A strategy

(b). B strategy

Figure 4. Inverter output side current.

(a). A strategy

(b). B strategy

Figure 5. THD of inverter output current.

4.2. NP potential balance capability analysis of DC bus.

The NP potential balance capability of the DC bus of the two algorithms is analyzed and compared. The DC midpoint potential and its potential difference are shown in Figure 6. FIG. 6(a) and (b) show the experimental results of the neutral voltage on the DC side of the two control strategies, whose average potential difference is about 0.5 and 0.3, respectively. Both model predictive control algorithms have good NP potential balance ability.
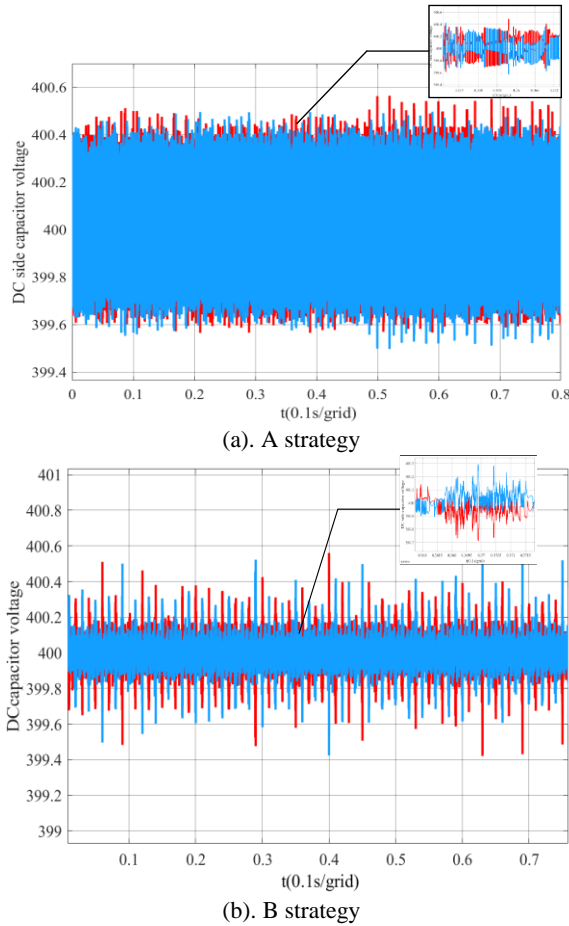

(a). A strategy

(b). B strategy

Figure 6. Midpoint potential and potential difference at DC side.

4.3. Dynamic response performance analysis

Figure 7 shows the current mutation experiment, which is used to verify the dynamic characteristics of the two improved algorithms. FIG. 7(a) shows the current jump, and the RMS value of the three-phase command current increases from 15A to 20A. FIG. 7(b) shows current attenuation, with the current decaying from 15A to 12A. Under both working conditions, the three-phase current can effectively track the command value. When the command current changes, the current can reach the command value in a very short time and ensure the stability of the system.
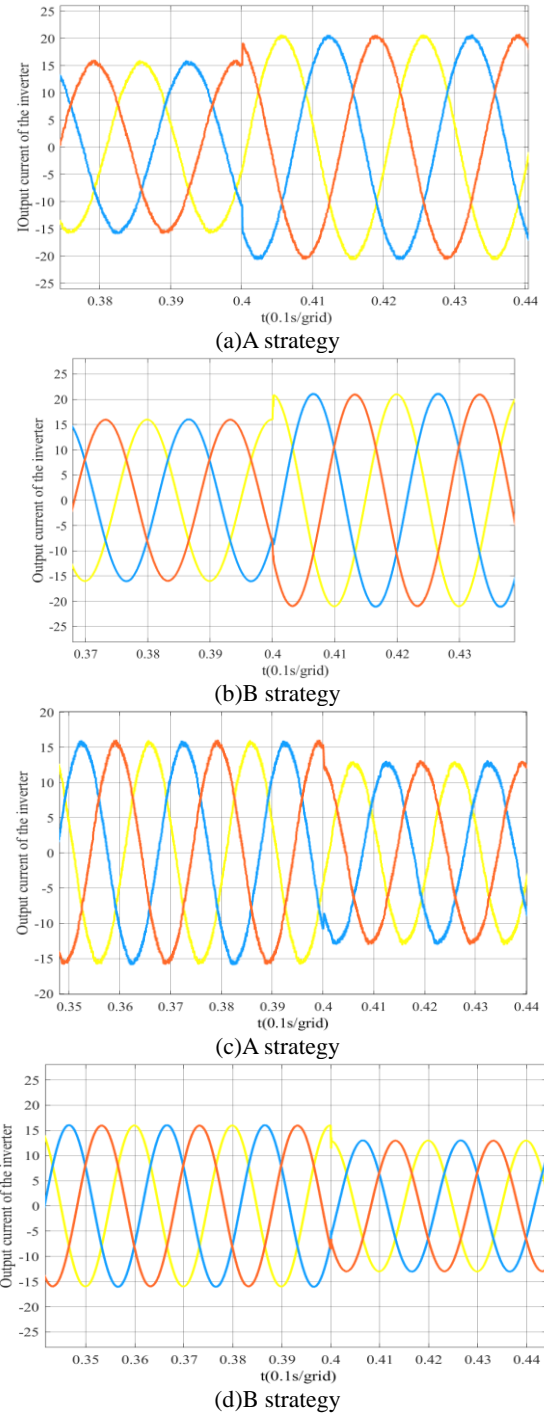

(a)A strategy

(b)B strategy

(c)A strategy

(d)B strategy

Figure 7. Current mutation experiment.

4.4. ESO compensation under inductance mismatch

The inductance mismatch experiment was carried out under the MPC strategy without ESO complement and the optimized MPC strategy. The static inductance value was 8mH, and the model inductance value was 4mH and 3mH, respectively. Observe the THD of the output current of the inverter, as shown in Figure 8 and 9. Because the inductance value of the model does not match, the harmonic component of the output current of the inverter is increased; Compensation can be effectively compensated through ESO.
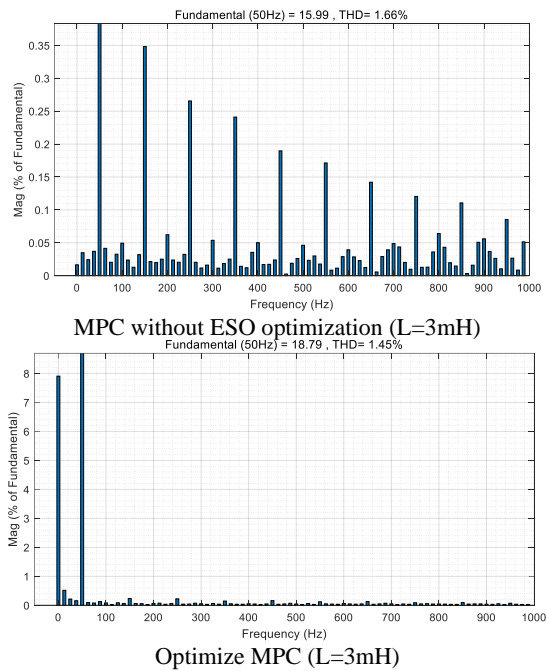
Fundamental (50Hz) = 15.99 , THD= 1.66%

MPC without ESO optimization (L=3mH)

Fundamental (50Hz) = 18.79 , THD= 1.45%

Optimize MPC (L=3mH)

Figure 8. Output current THD of inverter with mismatched inductance.

Fundamental (50Hz) = 15.99 , THD= 1.06%

MPC without ESO optimization(L=4mH)

Fundamental (50Hz) = 18.73 , THD= 0.94%
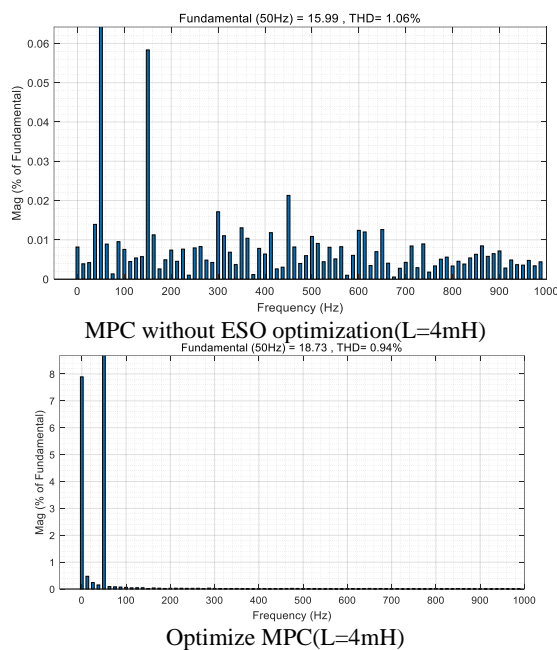
Optimize MPC(L=4mH)

Figure 9. Output current THD of inverter with mismatched inductance.

5 Conclusion

This paper takes T-type three-level grid-connected converter as the research object, and studies T-type three-level multi-optimization model predictive control strategy is studied. It mainly includes the control of output voltage control and NP-V as well as the optimization of switching state. It is verified by simulation, and verified by steady-state experiment and dynamic experiment. The model predictive control strategy based on multi-objective optimization has certain improvement in grid-connection performance and balanced DC neutral voltage. The effectiveness of ESO compensation is verified by inductance mismatch.

References

1. Kantar E, Hava A M. Optimal Design of Grid-Connected Voltage-Source Converters Considering Cost and Operating Factors[J].IEEE Transactions on Industrial Electronics, 2016, 63(9):5336-5347.DOI:10.1109/TIE.2016.2573759.

2. Schweizer M, Kolar J W. Design and Implementation of a Highly Efficient Three-Level T-Type Converter for Low-Voltage Applications[J].IEEE Transactions on Power Electronics, 2013, 28(2):899-907.DOI:10.1109/TPEL.2012.2203151.

3. Yang Y , Wen H , Fan M ,et al.Fast Finite-Switching-State Model Predictive Control Method Without Weighting Factors for T-Type Three-Level Three-Phase Inverters[J].Dianji yu Kongzhi Xuebao/Electric Machines and Control, 2019(3).DOI:10.1109/tii.2018.2815035.

4. Sang S , Cai X , Gao N ,et al.A Model Predictive Control Algorithm Applied in T-type Three-level Power Conversion System[C]//International Conference on Renewable Power Generation (RPG 2015).IET, 2015.DOI:10.1049/cp.2015.030.

5. Schweizer M , Lizama I , Friedli T ,et al.Comparison of the chip area usage of 2-level and 3-level voltage source converter topologies[C]//Conference of the IEEE Industrial Electronics Society.IEEE, 2010.DOI:10.1109/IECON.2010.5674994.

6. Choi U , Blaabjerg F , Lee K .Reliability Improvement of a T-Type Three-Level Inverter With Fault-Tolerant Control Strategy[J].IEEE Transactions on Power Electronics, 2015, 30(5):2660-2673.DOI:10.1109/TPEL.2014.2325891.

7. D. Zhang, L. Zhang, J. Jiang, J. Li, B. Wang and Z. Zhou, "Design of T-type three-level energy storage inverter and grid-connected control strategy," IECON 2017 - 43rd Annual Conference of the IEEE Industrial Electronics Society, Beijing, China, 2017, pp. 1072-1076, doi: 10.1109/IECON.2017.8216184.

8. Kumar N , Saha T K , Dey J .Sliding-Mode Control of PWM Dual Inverter-Based Grid-Connected PV System: Modeling and Performance Analysis[J].IEEE Journal of Emerging & Selected Topics in Power Electronics, 2016, 4(2):435-444.DOI:10.1109/JESTPE.2015.2497900.

9. S. Sang, N. Gao, R. Li and X. Cai, "A model predictive control algorithm applied in T-type three-level power conversion system," International Conference on Renewable Power Generation (RPG 2015), Beijing, 2015, pp. 1-6, doi: 10.1049/cp.2015.0301.

10. Cortes P , Kazmierkowski M P , Kennel R M ,et al.Predictive Control in Power Electronics and Drives[J].IEEE Transactions on Industrial Electronics, 2008, 55(12):4312-4324.DOI:10.1109/TIE.2008.2007480.

11. Yaramasu V , Wu B , Chen J .Model-Predictive Control of Grid-Tied Four-Level Diode-Clamped Inverters for High-Power Wind Energy Conversion Systems[J].IEEE Transactions on Power Electronics, 2014, 29(6):2861-2873.DOI:10.1109/TPEL.2013.2276120.

12. Abdel-Rahim O , Funato H .T-type three-level neutral point clamped inverter with model predictive control for grid connected photovoltaic applications[C]//Electrical Machines and Systems (ICEMS), 2016 19th International Conference on.IEEE, 2016.

13. M. Lak, B. -R. Chuang and T. -L. Lee, "An MVPWM based method for three-level T-type inverter with neutral point voltage balancing capability in the full range of power factor," *2021 IEEE 12th Energy Conversion Congress & Exposition - Asia (ECCE-Asia), Singapore, Singapore, 2021, pp. 920-925, doi: 10.1109/ECCE-Asia49820.2021.9479309.